Wireless Personal Communications (2023) 131:2173–2192
https://doi.org/10.1007/s11277-023-10537-7

Improved Detection Schemes for Non-coherent Pulse-Position Modulation

Hassan Khani[1]

Accepted: 21 May 2023 / Published online: 6 June 2023

Abstract
Energy-detection (ED) pulse-position modulation (PPM) receivers exhibit poor performance and low rates. Coherent receivers do not have such problems but their complexity is unacceptable. We propose two detection schemes to increase the performance of non-coherent PPM receivers. Unlike the ED-PPM receiver, the first proposed receiver cubes the absolute value of the received signal before demodulation and achieves a considerable performance gain. This gain is obtained because the absolute-value cubing (AVC) operation reduces the effect of low-SNR samples and increases the effect of high-SNR samples on the decision statistic. To further increase energy efficiency and rate of the non-coherent PPM receivers at almost the same complexity, we use the weighted-transmitted reference (WTR) system instead of the ED-based receiver. The WTR system has adequate robustness to weight coefficients and integration interval variations. To generalize the AVC concept to the WTR-PPM receiver, the reference pulse is first passed through a polarity-invariant squaring (PIS) operation and then is correlated with the data pulses. In this paper, the performance of different receivers employing the binary PPM (BPPM) is investigated at data rates of 2.08 and 9.1 Mbps over in-vehicle channels in the presence of noise, inter-block interference, inter-pulse interference, and inter-symbol interference (ISI). Simulations show that the proposed AVC-BPPM receiver outperforms the ED-based one in the absence of ISI and offers the same performance in the presence of strong ISI, the WTR-BPPM system considerably outperforms the ED-BPPM system (especially at high rates), and the proposed PIS-based WTR-BPPM system considerably outperforms the conventional WTR-BPPM system.

Keywords Absolute-value cubing · Energy detection · Polarity-invariant squaring · Pulse position modulation · Ultra-wideband · Weighted-transmitted reference

✉ Hassan Khani
h.khani@qiet.ac.ir

[1] Electrical and Computer Engineering Department, Quchan University of Technology, Quchan, Khorasan Razavi 9477177870, Iran

1 Introduction

Impulse radio (IR) ultra-wideband (UWB) communication systems employ ultra-narrow pulses with less than 1 ns duration for ranging and communications. They have attractive features, such as simplicity, precise ranging, high data rate, low latency, coexistence with current wireless systems, robustness to multipath, high penetration capability, and fine time resolution [1–4]. These features motivate the use of IR-UWB technology in low-latency real-time high-resolution positioning, short-range high-rate wireless connectivity, and tracking applications [5–9].

IR-UWB technology is promising for use in internet of things (IoT) [10], autonomous vehicles [5], navigation [11], robotics [12], smart logistics [2], medical applications [13], wireless body area networks [14], and wireless sensor networks [11]. Currently, Samsung Galaxy Note 20 Ultra uses UWB technology for both device-to-device connection and as a digital key for access control [8]. Also, Apple iPhones are equipped with a UWB chip for spatial awareness to accurately locate one another [8]. UWB ranging has been used for social distancing and contact tracing, especially during the COVID-19 pandemic [15]. Moreover, car manufacturers like Audi and BMW use UWB systems for keyless entry and hands-free access control [8].

Though transmitting short-duration pulses brings many interesting features for the UWB technology, it causes a crucial problem in the receiver design. The received IR-UWB signals contain many multipath components (MPCs) [16]. Estimating such a high number of MPCs makes the receiver implementation infeasible [16]. To exploit multipath diversity with low complexity and collect more energy from MPCs, several non-coherent IR-UWB receivers have been proposed [17–21].

Among the non-coherent IR-UWB receivers, the energy detection (ED) pulse position modulation (PPM) receivers are promising for applications demanding low-power consumption and low complexity [20, 21], such as IoT and robotics. However, the squaring operation in the ED-based receivers makes them vulnerable to noise plus interference and decreases their performance compared with the coherent receivers [20]. Moreover, in an ED-PPM receiver, the time spacing of the PPM modulation (a.k.a PPM parameter) should be greater than the maximum delay spread of the multipath channel, referred to as T_{mds}. In this way, inter-symbol interference (ISI) is avoided and high performance is assured. However, keeping the PPM parameter larger than T_{mds} comes at the expense of a severely reduced achievable data rate. Therefore, ED-PPM receivers exhibit poor performance and low data rates.

Coherent receivers such as matched-filter or rake receivers bypass the problems of the ED-PPM receivers. But, coherent receivers need full-channel state information, which makes their complexity impractical. In this paper, we propose two novel detection schemes for non-coherent PPM receivers to promote the performance of the non-coherent PPM receivers existing in the literature. The first scheme, referred to as absolute-value cubing (AVC), increases the performance of reference-free PPM detection schemes. The second scheme, denoted as polarity-invariant squaring (PIS), improves the performance of PPM detection schemes that use a noisy reference (dirty template). Unlike the ED-PPM receiver which squares the received signal, the proposed AVC receiver cubes the absolute value of the received signal before demodulation and achieves a considerable performance gain. This gain is obtained because the AVC operation increases the effect of the high-SNR samples in the decision variable compared to the squaring operation of the ED-based receivers.

To further increase the energy efficiency and rate of the non-coherent PPM systems at almost the same complexity, we propose to use the weighted-transmitted reference (WTR) system instead of the ED-based one. The WTR system moderates the main deficiencies of the conventional transmitted reference (TR) systems which are [22, 23]: (i) presence of harsh nonlinear ISI (ISI×ISI term) at high rates in the decision variable, (ii) low energy efficiency; (iii) low achievable data rates, and (iv) performance loss because of employing a noisy reference, which leads to the presence of a strong noise×noise term in the decision variable. Moreover, the WTR system has adequate robustness to variations of the weight coefficients and the integration interval. To generalize the AVC concept for the WTR-PPM receiver, the reference pulse is first passed through a PIS operation and then correlated with the data pulses. Unlike the squaring operation that omits the sign of the input, the PIS operation maintains the sign of the input and does not change it. For example, the output of the PIS device for 2 and −3 is equal to 4 and −9, respectively (the PIS device assigns 4–2 and −9 to −3). Hence, after correlating the PIS-operated reference pulse with the data pulses, the third power of the received signal is obtained similar to the cubing operation in the AVC approach. This paper shows that the WTR-based receivers, characterized as non-coherent receivers, perform better than the ED-based ones in multipath environments. This paper investigates the performance of different receivers employing the binary PPM (BPPM) at data rates of 2.08 and 9.1 Mbps over measured in-vehicle channels in the presence of noise, inter-block interference (IBI), inter-pulse interference (IPI), and ISI. Simulation results show that (i) the proposed AVC-BPPM receiver outperforms the ED-PPM one in the absence of ISI and offers the same performance in the presence of strong ISI, (ii) the WTR-BPPM system considerably outperforms the ED-BPPM system (especially at high rates), and (iii) the proposed PIS-based WTR-BPPM system considerably outperforms the conventional WTR-BPPM system.

1.1 Objective and Contributions

This paper aims to increase the BER performance of the non-coherent detection schemes existing in the literature with a marginal increase in the receiver complexity. The contributions of this paper are two-fold to address this objective: (i) an improved non-coherent receiver denoted as the AVC-PPM receiver is proposed to replace the conventional ED-PPM one to detect PPM signals without using any reference. The AVC-PPM receiver uses the absolute value of the cubed received signal instead of the squared one used in the conventional ED-PPM receiver, and (ii) an improved WTR-PPM receiver, referred to as the PIS-based WTR-PPM receiver, is proposed to generalize the AVC concept to the TR receivers, which use a noisy reference (dirty template) for detection. The PIS-based WTR-PPM receiver squares the reference pulse samples while maintaining their sign, and then correlates the resultant reference pulse with the data pulses.

1.2 Literature Survey

Conventional ED-PPM receivers are widely used in the literature [20, 21, 24–30]. An improved pulse position modulation, known as multipulse PPM, is proposed in [31] to achieve a higher bit rate and bandwidth efficiency for PPM communication systems. In [32], this modulation scheme is applied to a UWB communication system using an energy detector, where 1.33 to 2.5 bits are transmitted per pulse (the conventional ED-BPPM which transmits one bit per pulse). The PPM receivers in [33] and [34] use the envelope

(absolute value) of the received signal while the PPM receiver in [35] uses the peak value of the envelope of the received signal for detection. Note that using the envelope for detection simplifies the receiver design at the expense of a severe performance loss. To reduce narrowband interference in ED-PPM receivers, [20] proposes the Teager-Kaiser operator, while [21] proposes a nonlinear blind technique with much lower complexity and almost the same performance. In [36], compressed sensing is employed for ED-PPM using the sparsity of the UWB channels at the expense of an increase in receiver complexity. In [17–19], the TR-PPM receiver is proposed which correlates the reference pulse with the data pulses for detection. The maximum ratio combing receiver is used in [37] for detecting BPPM signals in the presence of noise, multi-access interference, and IPI. Other coherent detection schemes for PPM signals are investigated in [38] and [39] without considering path-dependent pulse distortion of UWB channels. CMOS-based UWB transceiver design for PPM is done in [34], which achieves a rate of 1.125 Gbps over a 2 m distance. Since the use of PPM in deep-space optical communication is becoming a hot research topic, [40–42] consider PPM optical communication. Moreover, the multipulse PPM has been recently used for ultraviolet communications [43]. Note that the output of optical or ultraviolet detectors is proportional to the energy of the incident beam. Therefore, the proposed AVC-PPM detection scheme can also be used in optical and ultraviolet communications. Employing the PPM scheme, [19] considers joint communication and radar, and [35] investigates joint information and power transfer. Moreover, covert communication using PPM is proposed in [44], and space-time code design using ED-PPM detectors is investigated in [29, 30]. Table 1 compares different detection methods for PPM in terms of complexity and performance.

Simulation results show that the proposed AVC-PPM and the PIS-based WTR-PPM receivers offer much better BER performance over the ED-PPM and the conventional WTR-PPM receivers, respectively, over realistic in-vehicle UWB channels measured in [45].

Following this introduction, Sect. 2 models the ED-BPPM, the proposed AVC-BPPM, the conventional WTR-BPPM, and the proposed PIS-based WTR-BPPM systems. The origin of the performance improvement of the AVC operation in non-coherent PPM detection is intuitively analyzed and numerically validated in Sect. 3. Section 4 evaluates the uncoded BER performance for different receivers through simulations over measured line-of-sight (LOS) and non-LOS (NLOS) in-vehicle UWB channels. Finally, Sect. 5 concludes this paper and provides future directions. Table 2 describes the mathematical symbols used throughout this paper.

2 System Models

To simplify notation, multiple access schemes are neglected throughout this paper. Moreover, it is assumed that each bit is transmitted by a single UWB pulse, and receivers are perfectly synchronized.

2.1 Energy Detection BPPM Receiver

The system structure of an ED-PPM receiver is shown in Fig. 1. First, a low-noise amplifier amplifies the received signal, and then, a bandpass filter (BPF) removes the

Table 1 Comparison of different PPM detection schemes

Reference(s) Number	Detection method	Complexity	Performance
[33, 34]	Using the absolute value of the received signal	Very low	Very low
[35]	Using the peak value of the received signal envelope	Very low	Very low
[36]	Energy detection + compressed sensing	Moderate	Moderate
[24–30]	Energy detection for conventional PPM scheme	Low	Moderate
[32]	Energy detection for enhanced PPM scheme	Moderate	Moderate (better than conventional ED-BPPM)
[17–19]	Correlating the reference pulse with data pulses (TR)	High	Moderate (better than ED-PPM)
[38, 39]	Coherent detection	Very high	Best
This paper (AVC-PPM)	Cubing the absolute value of the received signal	Low	Better than ED-PPM
This paper (PIS-based WTR-PPM)	Squaring the transmitted-reference pulse without losing its sign, then correlating the result with data pulses	High	Better than the conventional WTR-PPM

out-of-band noise and interference. Next, the received bandpass filtered signal, $r(t)$, passes through the ED device followed by a sampler and information detector.

The ED-based receivers detect the information by comparing the energy of the received signal in predefined intervals. To have no IPI and ISI, the duration of the intervals should be greater than or equal to T_{mds}. We express the signal at the output of the BPF by:

$$r(t) = \sum_{j=-\infty}^{\infty} g(t - jT_s - b_j\delta) + n(t) = s(t) + n(t) \tag{1}$$

where $g(t) = w_{tr}(t) * C(t) * f(t)$ is the received noise-free pulse ($w_{tr}(t)$ is the transmitted bandpass UWB pulse with a bandwidth W and a center frequency f_c, $C(t)$ is the multipath channel impulse response, and $f(t)$ shows the BPF impulse response). In (1), $s(t)$ is the received noise-free bandpass filtered UWB signal and $n(t)$ shows the bandpass filtered additive white Gaussian noise (AWGN) with a two-sided power spectral density $\frac{N_0}{2}|F(f)|^2$, where $|x|$ indicates the absolute value of x and $F(f)$ denotes the Fourier transform of $f(t)$. Moreover, T_s denotes the symbol duration; $b_j \in \{0, +1\}$ represents the jth information bit; and δ is the PPM parameter. To demodulate the jth information bit, the received signal is squared and integrated from jT_s to $jT_s + T_i$ and from $jT_s + \delta$ to $jT_s + T_i + \delta$. Then, the output of the integrator is sampled and the former sample is subtracted from the latter one. Finally, the subtraction result is applied to a unit step function. Thus, in the conventional ED-BPPM receiver, the integration output for the jth information bit is expressed as:

$$z_i[j] = \int_0^{T_i} r^2(t + jT_s + i\delta)dt, \; i \in \{0, 1\} \tag{2}$$

and finally, the jth information bit is detected as follows:

Table 2 Definition of mathematical symbols

Notation	Definition
μ	Mean of a random variable
σ	The standard deviation of a random variable
$w_{tr}(t)$	Transmitted UWB pulse
$C(t)$	The impulse response of the multipath channel
$f(t)$	The impulse response of the receiver front-end bandpass filter
$F(f)$	Fourier transform of $f(t)$
$*$	Linear convolution operator
$g(t)$	Received noise-free bandpass filtered signal when $w_{tr}(t)$ is sent, i.e., $g(t) = w_{tr}(t) * C(t) * f(t)$
$s(t)$	Received noise-free bandpass filtered signal
$n(t)$	Bandpass filtered additive white Gaussian noise at the output of the receiver front-end bandpass filter
b	Transmitted bit
$\hat{b}$	Estimate of the transmitted bit b
N_0	One-sided power spectral density of the noise in the communication channel
T_s	Symbol dusration in ED-PPM and AVC-PPM systems/ Time spacing between consecutive data pulses in WTR-PPM systems
T_i	The length of the integration interval
$\|x\|$	The absolute value of x
α	Weight of the reference pulse in WTR systems
β	Weight of the data pulses in WTR systems
N_s	Number of data pulses per block in WTR systems
T_d	Guard time between the reference pulse and data pulses in WTR systems
T_B	Block length in WTR systems
T_{mds}	Maximum delay spread of the channel
$u(t)$	Unit step function defined as: $u(t) = \begin{cases} 1, & t \geq 0 \\ 0, & t < 0 \end{cases}$
$sign(t)$	Modified signum function defined as: $sign(t) = \begin{cases} +1, & t \geq 0 \\ -1, & t < 0 \end{cases}$

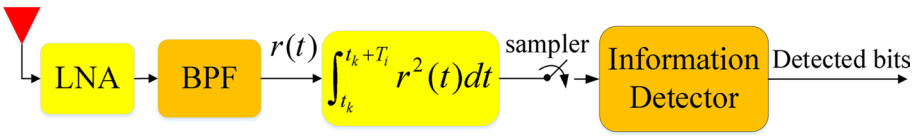

Fig. 1 Structure of the ED-PPM receiver

$$\hat{b}_j = u(z_1[j] - z_0[j]). \tag{3}$$

where $u(t)$ indicates the unit step function.

2.2 Proposed Absolute-Value Cubing BPPM Receiver

The structure of an absolute-value cubing (AVC) PPM receiver is illustrated in Fig. 2. Note that the structure of the AVC-BPPM receiver is the same as that of the ED-BPPM one except that the filtered received signal is fed to the AVC device instead of the squaring device.

Since high-SNR samples are very likely to have a larger amplitude than the low-SNR ones, the AVC device increases the contribution of the high-SNR samples to the decision variable compared with the squaring device. This is intuitively and numerically shown in Sect. 3. Hence, the AVC receiver shows more capability for small-sample removal than the ED receiver and consequently provides better performance than the ED receiver. Note that the calculation burden and complexity of the AVC-BPPM receiver are almost the same as those of the ED-BPPM one.

2.3 Conventional WTR-BPPM Receiver

A WTR system transmits data block-wise. If each data pulse carries one information bit, each block consists of $N_s + 1$ pulses. In this case, the first pulse in each block is the reference pulse which is followed by N_s data pulses closely spaced in time as shown in Fig. 3. To prevent IBI and have an interference-free reference, a guard time T_d is inserted between the reference pulse and the data pulses as seen in Fig. 3. Moreover, by assigning a larger amplitude to the reference pulse than to the data pulses, the SNR of the reference pulse which plays an important role in detection increases. Thus, we can express the transmitted signal of the WTR-PPM system by:

$$s_{tr}(t) = \sum_{j=-\infty}^{\infty} \left\{ \alpha w_{tr}(t - jT_B) + \beta \sum_{i=0}^{N_s-1} w_{tr}(t - jT_B - iT_s - b_{j,i}\delta - T_d) \right\} \tag{4}$$

where N_s is the number of data pulses per block, $T_B = 2T_d + (N_s - 1)T_s + \delta$ shows the block length, T_d shows the guard time between the reference pulse and the preceding/succeeding data pulses, and T_s is the time spacing between two successive data pulses. Also, α and β respectively denote the weights of the reference pulse and data pulses. Finally, $b_{j,i} \in \{0, +1\}$ shows the ith information bit of the jth block. To have a fair comparison between weighted and unweighted systems, the following equation should be satisfied:

$$\alpha^2 + N_s\beta^2 = N_s. \tag{5}$$

The structure of the conventional WTR-BPPM receiver is depicted in Fig. 4. First, the received signal passes through the BPF. The signal at the output of the BPF is written as:

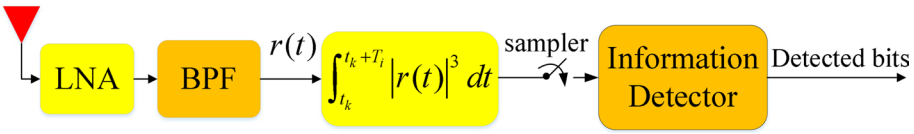

Fig. 2 Structure of the proposed AVC-PPM receiver

$$r(t) = \sum_{j=-\infty}^{\infty} \left\{ \alpha g(t - jT_B) + \beta \sum_{i=0}^{N_s-1} g(t - jT_B - iT_s - b_{j,i}\delta - T_d) \right\} + n(t); \quad = s(t) + n(t), \tag{6}$$

Without loss of generality, we focus on the demodulation of the first block. To detect the kth bit of the block, we multiply the received signal $r(t)$ by $r(t + kT_s + T_d)$ and $r(t + kT_s + T_d + \delta)$. Then, we integrate these two multiplications and sample the output of the integrators. Next, as shown in Fig. 4, the upper sample is subtracted from the lower one and the result is applied to a unit step function. The output of the integrators for the kth bit of the block in the conventional WTR-PPM receiver is:

$$z_i[k] = \int_0^{T_i} r(t)r(t + kT_s + T_d + i\delta)dt, \; i \in \{0, 1\} \tag{7}$$

Finally, the kth bit of the block is detected by a unit step function as follows:

$$\hat{b}_k = u(z_1[k] - z_0[k]). \tag{8}$$

2.4 Proposed Polarity-Invariant Squaring-Based WTR-BPPM Receiver

The structure of the PIS-based WTR-BPPM receiver is illustrated in Fig. 5. Comparing Fig. 4 with Fig. 5 shows that the structure of the PIS-based WTR-BPPM receiver is the same as that of the conventional WTR-PPM one except that the reference pulse is first passed through the PIS device and then is used for demodulation. The PIS device squares the reference pulse and keeps its sign/polarity. In other words, the PIS device squares the reference pulse without altering its sign. For instance, if 2 and -3 pass through the PIS device, it outputs 4 and -9, respectively.

Squaring operation decreases the effect of the low-SNR (noise-dominant) samples and increases the effect of high-SNR samples of the reference pulse on the decision variable. Thus, the PIS operation shows small (low-SNR) sample removal capability and thereby offers superior performance. Note that the calculation required by the PIS device can be done with a square-law device, a sign detector, and a mixer (multiplier). Hence, the complexity of the new receiver is almost the same as the original one.

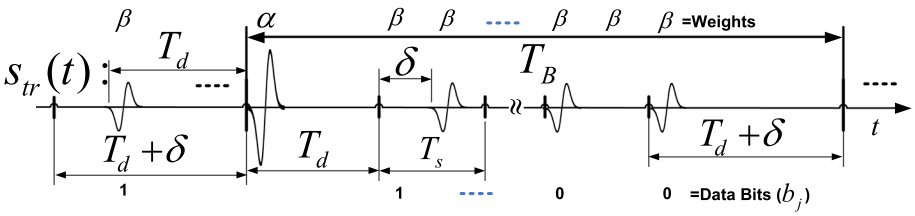

Fig. 3 A typical transmitted signal of the WTR-BPPM system

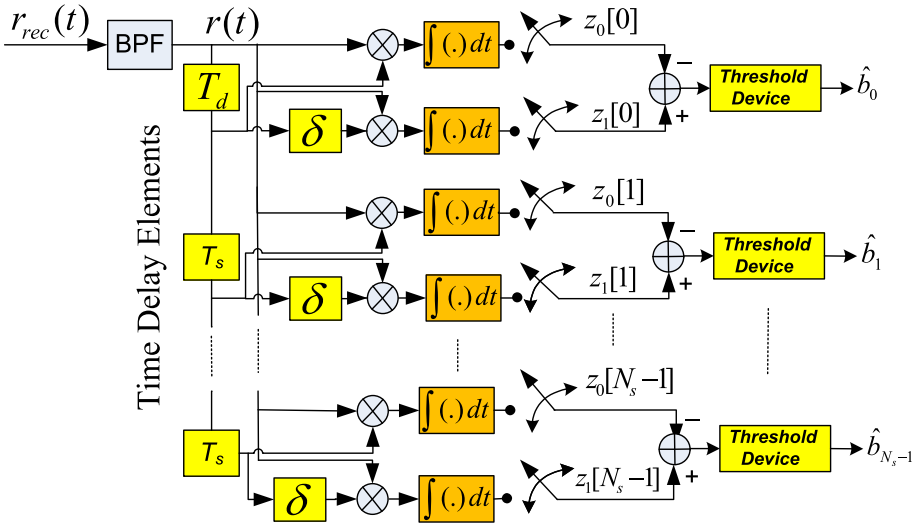

Fig. 4 The receiver diagram of the conventional WTR-BPPM system

3 How the AVC Operation Improves the Performance: Intuitive Analysis and Numerical Validation

In this section, we answer the following question through intuitive analysis and numerical calculations: how does absolute-value cubing (AVC) improve the BER performance in non-coherent PPM detection? To answer this question, first, we show that correlating the PIS-operated reference pulse with the data pulses is almost equivalent to the AVC operation. Denoting the received bandpass filtered signal by $r(t)$ and stating from the term under integral in the PIS-based WTR-PPM receiver, we end up with the term under integral in the AVC-PPM receiver as follows:

$$\begin{aligned} &\overbrace{sign(r(t))r^2(t)}^{\text{PIS-Operated Reference Pulse}} \times r(t) = sign(r(t))r^3(t) = sign(r(t))sign(r(t))|r(t)|^3 \\ &= sign^2(r(t))|r(t)|^3 = |r(t)|^3 \end{aligned} \tag{9}$$

where $sign(x)$ indicates the modified signum function. The last equality in (9) is obtained because $sign^2(x) = 1$.

In moderate to high-SNR range, high-SNR samples are very likely to have larger amplitudes than the low-SNR samples. Therefore, cubing the received noisy signal amplifies the high-SNR samples much more than the low-SNR samples. Thus, cubing the received signal or its absolute value magnifies the amplitude difference between the high-SNR samples and low-SNR samples. As a result, the proposed detection schemes reduce the effect of small (noise-dominant) samples and increase the effect of high-SNR samples on the

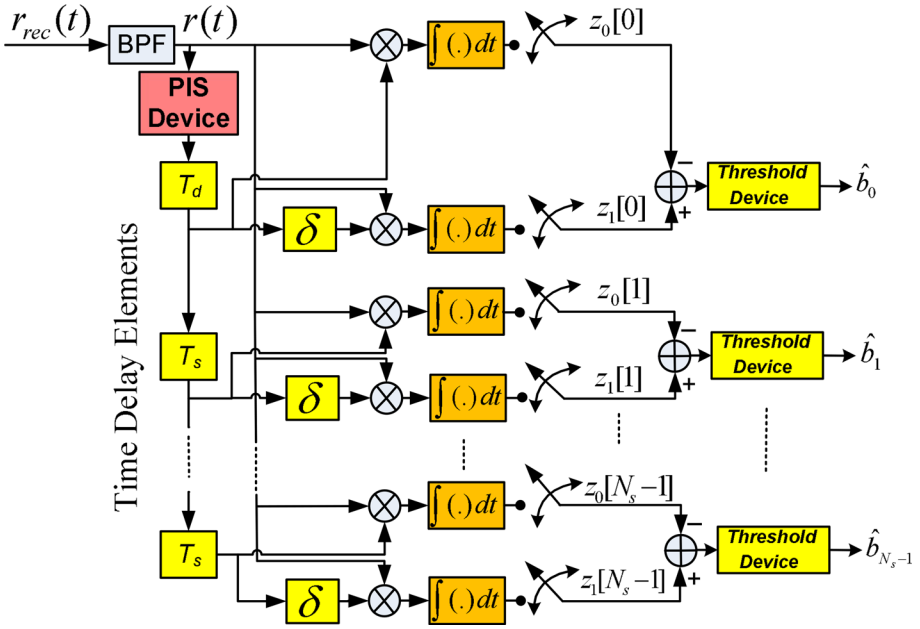

Fig. 5 The receiver diagram of the proposed PIS-based WTR-BPPM system

decision variable. In the ED-based detection of PPM signals, the energy difference between the signal plus noise interval and the pure-noise interval affects the receiver performance. The more energy difference (distance) is, the better performance is obtained. Therefore, cubing the signal or its absolute value offers better performance than squaring the signal because it magnifies the distance between decision hypotheses. Figure 6 intuitively shows the effect of squaring and absolute-value cubing on the amplitude of pure-noise, low-SNR, and high-SNR samples. In this figure, we consider a zero-mean AWGN with a standard deviation (SD) of 2/3. We remark that the value of a normal random variable with mean μ and SD σ is between $\mu - 3\sigma$ and $\mu + 3\sigma$ with a chance of 99.73%. Hence, the value of the considered normal noise is between -2 and 2 with a chance of 99.73%. Similarly, if the value of the signal is a, the value of the considered noise plus signal is between a-2 and a+2 with a chance of 99.73%. In Fig. 6, this range of values for the noisy signal (signal + noise) is depicted by a red line on the left side of the noise-free sample which is shown by a blue dot. In this figure, R_1 denotes the amplitude ratio of the high-SNR sample to the low-SNR sample and R_2 indicates the amplitude ratio of the high-SNR sample to the pure-noise sample in the worst case (i.e., considering the minimum value for the high-SNR sample and the maximum value for the low-SNR and pure-noise samples). It is seen that R_1 and R_2 increase with the signal exponent. Since the noise-free sample is not located in the center of the noisy-signal range and is closer to the minimum value of the noisy signal, the skewness of the noisy signal is to the right which is seen in Fig. 7. To further validate the observations drawn from Fig. 6, the statistical mean of different types of samples are compared in Fig. 7 using a zero-mean AWGN vector of length 10000000 with an SD 2/3. This figure also illustrates the SD and histogram of different types of samples. Henceforth, we show the ratio of the high-SNR sample mean to the low-SNR sample mean by R_{hl}, the ratio of the high-SNR sample mean to the pure-noise sample mean by R_{hn}, and the ratio of the

low-SNR sample mean to the pure-noise sample mean by R_{ln}. Table 3 compares the values of R_{hl}, R_{hn}, and R_{ln} for different exponents by using the values given in Fig. 7. It is seen that R_{hl}, R_{hn}, and R_{ln} increase with the signal exponent, and R_{hn}, R_{hl}, and R_{ln} have the highest increment rate in descending order. From Fig. 7, it is also seen that the skewness of the noisy sample is to the right which increases with the signal exponent and decreases with SNR. One may conclude that increasing the signal exponent will improve the performance endlessly. However, increasing the signal exponent lessens the contribution of low-SNR samples and in the extreme case, the detection will rely on only one sample (the highest-SNR sample). In this case, the information in other samples is not taken into account and time diversity is not utilized. Therefore, theoretically and practically there is an end to

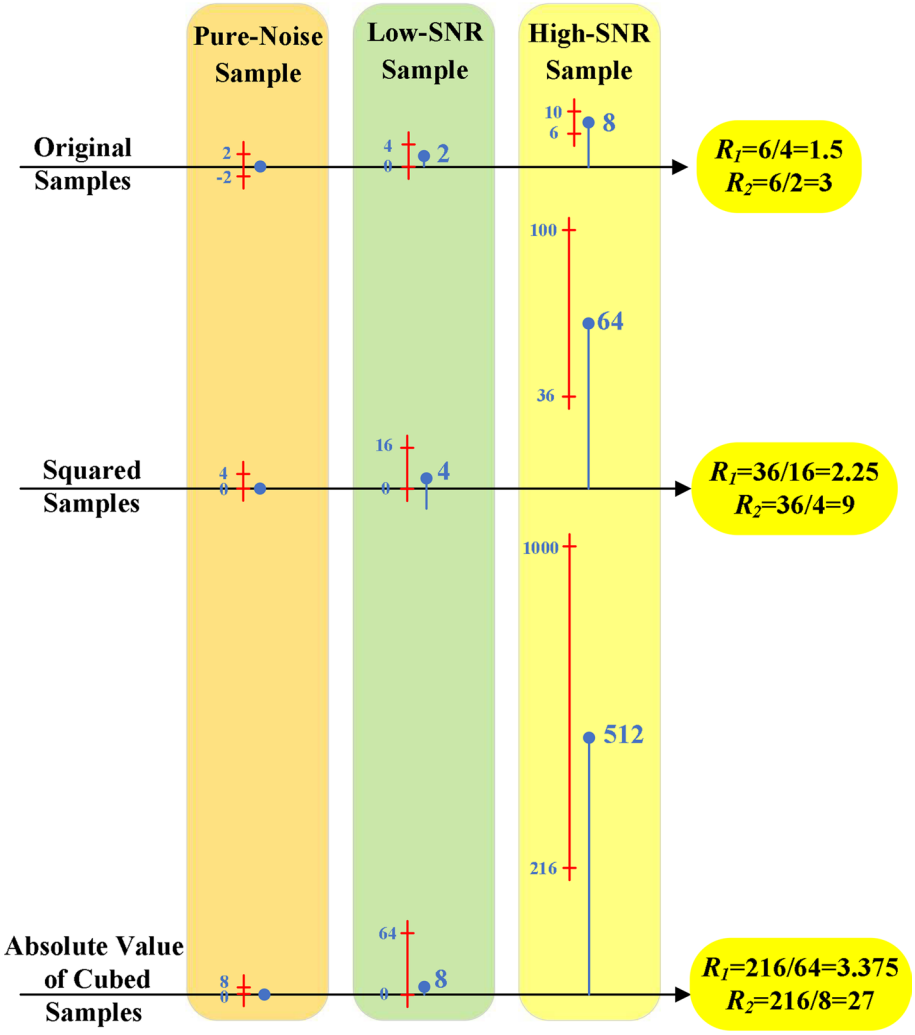

Fig. 6 The effect of squaring and absolute-value cubing on three types of samples, i.e., pure-noise (left column), low-SNR (center column), and high-SNR (right column) samples

the performance improvement caused by increasing the signal exponent in non-coherent detection schemes. There are other limitations for the proposed schemes: (i) when coherent detection schemes are used or (ii) when the detection is based on only one sample or (iii) when the amplitude of the received signal is lost due to monobit quantization, or (iv) when the SNR is below a certain threshold (the signal is buried in the noise), the proposed schemes do not offer any performance gain.

4 Simulation Results and Discussions

This section investigates the uncoded BER performance for the conventional ED-PPM, the AVC-PPM, the conventional WTR-PPM, and the PIS-based WTR-PPM receivers in measured LOS and NLOS in-vehicle channels [45] through computer simulations employing binary PPM (BPPM) modulation, taking into account noise, IPI, ISI, and IBI.

The transmitted pulse is a bandpass UWB pulse whose center frequency and 10 dB bandwidth are 3.35 GHz and 500 MHz, respectively. Simulations show that the estimate of the optimal value for β/α is about 0.625 for the WTR-PPM receivers. Therefore, we use $\beta/\alpha = 0.625$ in this paper. Simulation results are obtained by assuming perfect synchronization for receivers. Table 4 summarizes the simulation parameters.

Figures 8 and 9 compare the BER performance of different receivers for a low-rate case ($R_b = 2.08$ Mbps) in LOS and NLOS scenarios, respectively. Note that the AVC-PPM and PIS-based WTR-PPM receivers outperform the conventional ED-PPM and conventional

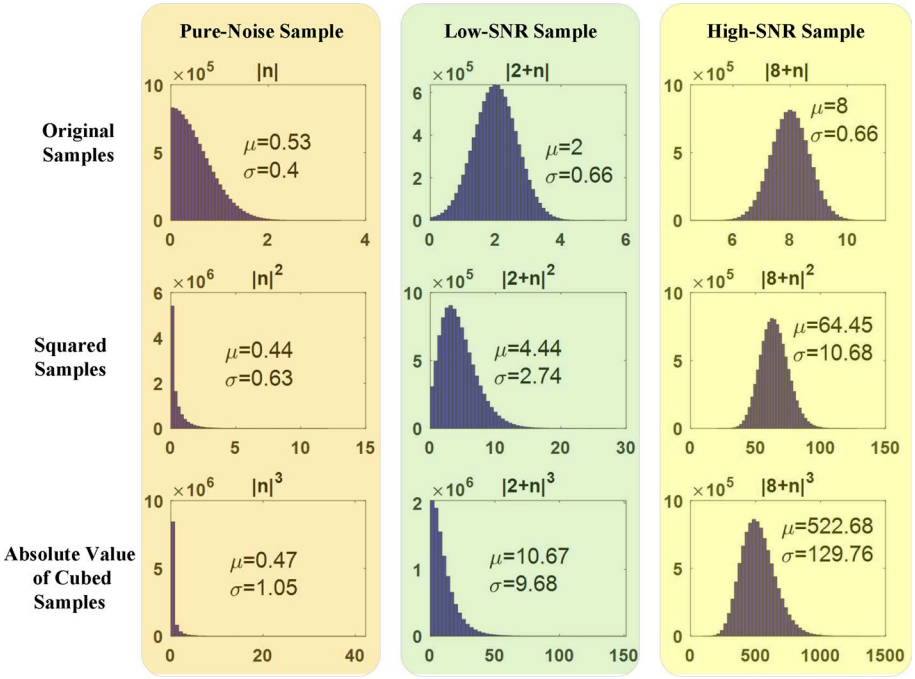

Fig. 7 The effect of squaring and absolute-value cubing on the mean, SD, and histogram of three types of samples, i.e., pure-noise (left column), low-SNR (center column), and high-SNR (right column) samples

Table 3 Comparison of R_{hl}, R_{hn}, and R_{ln} for Different Exponents

Exponent	R_{hl}	R_{hn}	R_{ln}
1 (original)	$8/2 = 4$	$8/0.53 = 15.01$	$4/0.53 = 7.55$
2 (squaring)	$64.45/4.44 = 14.52$	$64.45/0.44 = 146.48$	$4.44/0.44 = 10.09$
3 (AVC)	$522.68/10.67 = 48.96$	$522.68/0.47 = 1112.1$	$10.67/0.47 = 22.7$

WTR-PPM receivers, respectively. The PIS-based WTR-PPM, conventional WTR-PPM, AVC-PPM, and ED-PPM receivers have the best performance in descending order. In other words, the PIS-based WTR-PPM receiver offers the best performance and the ED-PPM receiver has the worst performance. Moreover, Figs. 8 and 9 show that at $BER = 10^{-3}$, the proposed AVC-PPM and PIS-based WTR-PPM receivers outperform their corresponding conventional receivers (ED-PPM and conventional WTR-PPM) by about 1 dB and 0.8 dB in LOS and NLOS scenarios, respectively. Note that the performance gain brought by the AVC-PPM and the PIS-based WTR-PPM decreases in NLOS channels because these receivers reduce the effect of the low-SNR samples and the number of such samples is larger in the LOS channels compared to the NLOS ones. As seen in Figs. 8 and 9, the WTR-PPM receivers considerably outperform the AVC-PPM and the ED-PPM receivers in both LOS and NLOS scenarios. This is because WTR-PPM receivers are more capable to distinguish between noise and the desired signal by employing a reference pulse despite this reference pulse is noisy.

Figures 10 and 11 illustrate the BER performance of different receivers for a high-rate case ($R_b = 9.1$ Mbps) for LOS and NLOS scenarios, respectively. Note that the ED-PPM and AVC-PPM receivers fail to detect information bits because the ISI is no longer negligible at high rates and these receivers cannot distinguish the desired signal from noise plus interference. However, the WTR-PPM receivers can recognize the desired signal from noise plus interference by using a noisy reference pulse and consequently, provide superior performance. It is seen that at BER=10^{-3}, the PIS-based WTR-PPM receiver outperforms the conventional WTR-PPM one by 1.5 dB and 1 dB in LOS and NLOS channels, respectively. Again, because of the larger number of low-SNR samples in LOS channels, the performance gain of the proposed PIS-based WTR-BPPM receiver is higher in such channels. Comparing Figs. 8 and 9 with Figs. 10 and 11 shows that the PIS-based WTR-PPM receiver offers higher improvement in higher rates because (i) the PIS-based WTR-PPM receiver reduces the effect of the low-SNR samples and increases the effect of high-SNR samples on the decision statistic and thereby greatly reduces noise and interference, (ii) the

Table 4 Simulation parameters

Parameter	Value
T_d	200 ns
T_s	200 ns or 15 ns
δ	100 ns or 7.5 ns
T_B	2400 ns or 550 ns
T_i	200 ns or 15 ns
R_b	2.08 Mbps or 9.1 Mbps
β/α	0.625

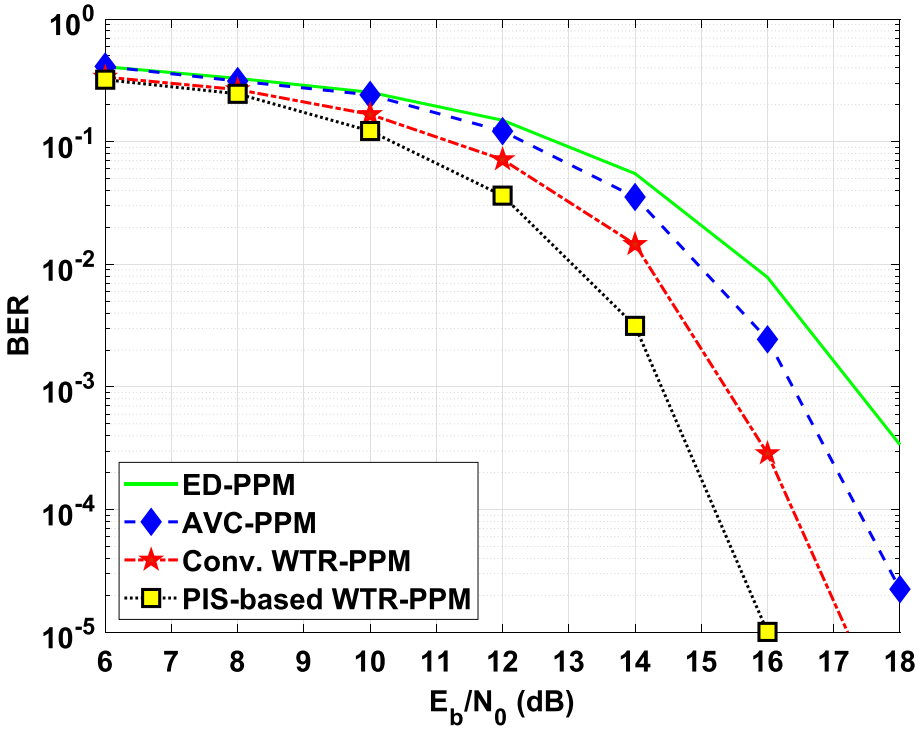

Fig. 8 Performance comparison of different binary receivers in LOS scenario for a low-rate case, i.e. $R_b = 2.08$ Mbps

amplitude of the reference pulse is larger than that of the data pulses in the WTR systems. Hence, the WTR-PPM receivers specifically the PIS-based one assures higher SNR for the reference pulse as the cornerstone of detection and thereby provides reliable performance even in channels with strong ISI.

5 Conclusions and Future Works

This paper proposed two novel non-coherent detection schemes to improve the BER performance of non-coherent PPM receivers existing in the literature. The proposed receivers achieve better performance by decreasing the effect of low-SNR samples and increasing the effect of high-SNR samples on the decision statistic. The first proposed scheme, denoted as AVC, cubes the absolute value of the received signal instead of squaring it (squaring is done in ED-PPM receivers). The second proposed technique, referred to as PIS, is applied to the WTR-PPM receiver. This scheme squares the reference pulse while maintaining its sign, and then correlates it with data pulses. The performance of the ED-PPM, AVC-PPM, WTR-PPM, and PIS-based WTR-PPM receivers have been investigated in measured LOS and NLOS in-vehicle channels for low-rate and high-rate modes of operation through simulations, taking into account noise, ISI, and IBI for binary PPM (BPPM). Among all receivers, the PIS-based WTR-PPM receiver

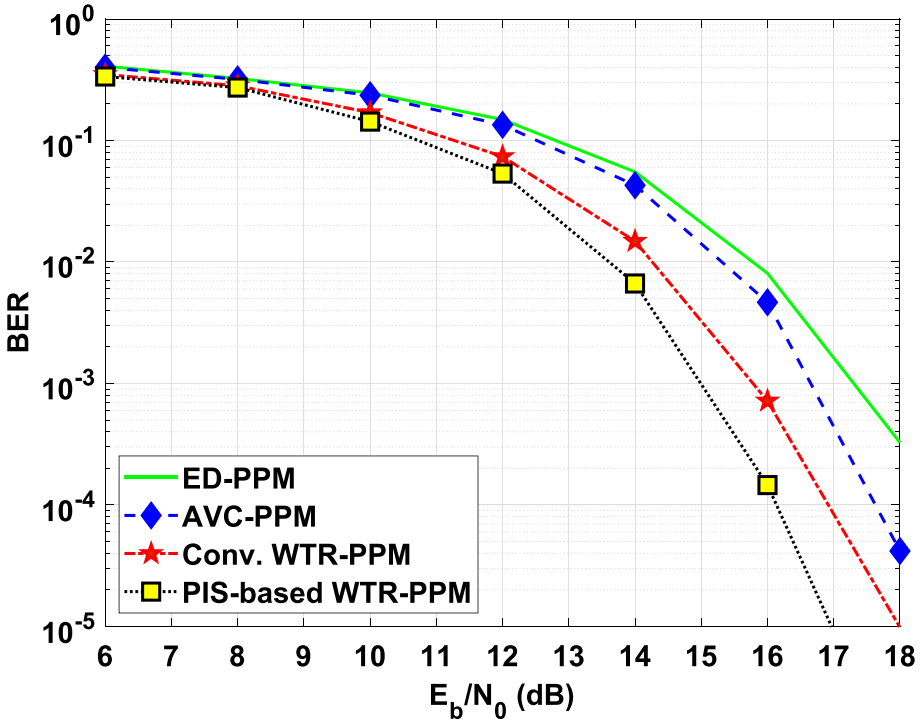

Fig. 9 Performance comparison of different binary receivers in NLOS scenario for a low-rate case, i.e. $R_b = 2.08$ Mbps

offers the best performance and the ED-PPM receiver has the worst performance. Since the number of low-SNR samples is larger in LOS channels, the performance gain of the proposed receivers is larger in LOS channels. Moreover, the ED-PPM and AVC-PPM receivers fail to detect information bits at high rates because they cannot distinguish the desired signal from noise plus interference. However, the PIS-based WTR-PPM receiver offers a larger gain in higher rates because on one hand, it reduces the effect of the low-SNR samples and increases the effect of high-SNR samples on the decision statistic. As a result, it greatly reduces noise and interference. Hence, the PIS-based WTR-PPM receivers increase the SNR of the reference pulse as the golden key for detection and thereby provide reliable performance even in the presence of strong ISI. Future research includes applying the proposed non-coherent techniques to non-UWB systems, non-binary PPM systems, and other non-coherent demodulation schemes that use no reference (e.g. on-off keying) or use noisy reference (dirty template). The AVC approach can be applied to the multipulse PPM system proposed in [31] or the multi-level PPM systems proposed in [25, 27, 28] for nanocommunications in Terahertz technology to achieve better BER performance. Moreover, using the proposed AVC-PPM instead of the ED-PPM is promising to increase the energy efficiency and positioning accuracy of the UWB ranging and localization systems.

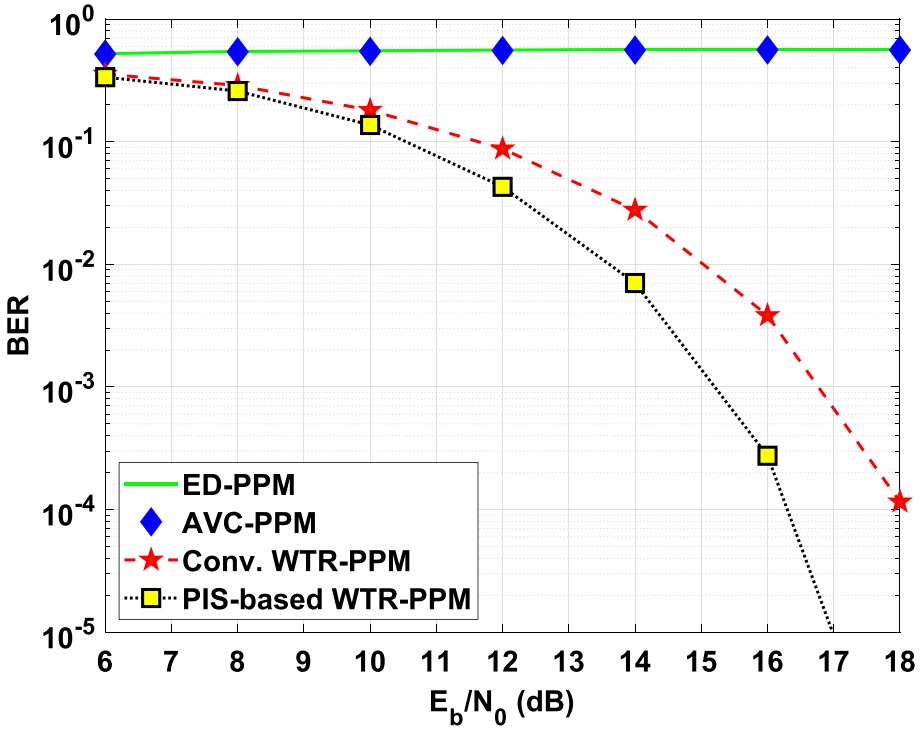

Fig. 10 Performance comparison of different binary receivers in LOS scenario for a high-rate case, i.e. $R_b = 9.1$ Mbps

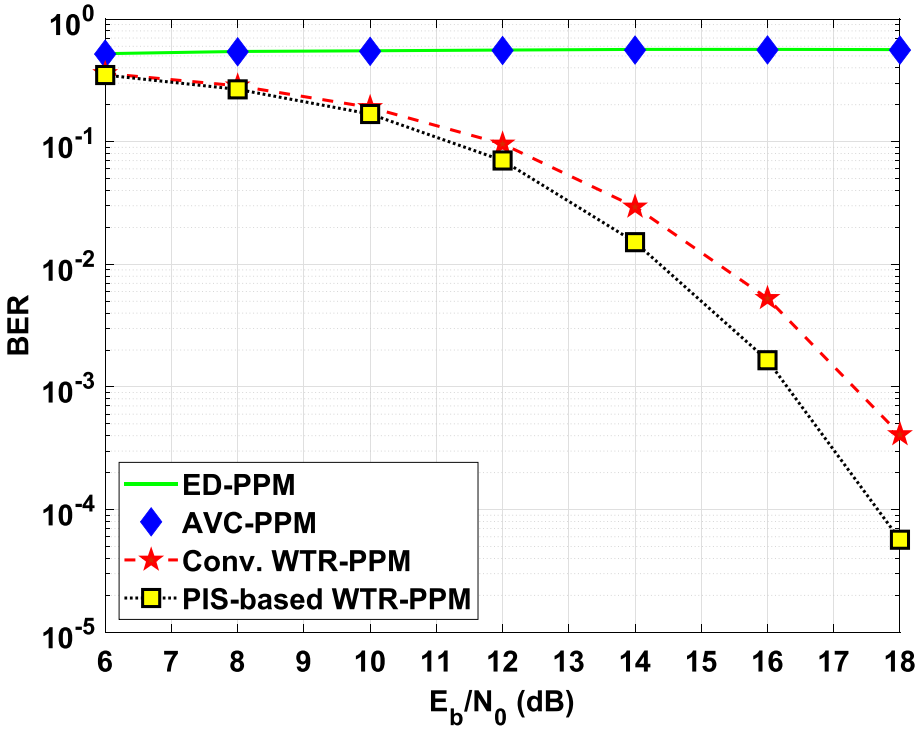

Fig. 11 Performance comparison of different binary receivers in NLOS scenario for a high-rate case, i.e. $R_b = 9.1$ Mbps

Author Contributions Not applicable.

Funding This work is supported by the Quchan University of Technology under Grant No. 95/5012.

Data Availability Data and materials of this article are available upon request (hassan.khani@gmail.com)

Code availability Matlab codes of this article are available upon request (hassan.khani@gmail.com).

Declarations

Conflict of interest The author has no conflict of interest/competing interests to declare that are relevant to the content of this article.

Ethical approval Not applicable.

Consent to participate Not applicable.

Consent for publication Not applicable.

References

1. Dardari, D., Chong, C.-C., & Win, M. (2008). Threshold-based time-of-arrival estimators in UWB dense multipath channels. *IEEE Transactions on Communications, 56*(8), 1366–1378. https://doi.org/10.1109/TCOMM.2008.050551
2. Elsanhoury, M., et al. (2022). Precision positioning for smart logistics using ultra-wideband technology-based indoor navigation: A review. *IEEE Access, 10*, 44413–44445. https://doi.org/10.1109/ACCESS.2022.3169267
3. Wang, J., et al. (2022). Multi-classification of UWB signal propagation channels based on one-dimensional wavelet packet analysis and CNN. *IEEE Transactions on Vehicular Technology*. https://doi.org/10.1109/TVT.2022.3172863
4. Shan, F., et al. (2022). Ultra-wideband swarm ranging protocol for dynamic and dense networks. *IEEE/ACM Transactions on Networking*. https://doi.org/10.1109/TNET.2022.3186071
5. Yang, B., et al. (2022). High-precision UWB-based localisation for UAV in extremely confined environments. *IEEE Sensors Journal, 22*(1), 1020–1029. https://doi.org/10.1109/JSEN.2021.3130724
6. Venkata Lakshmi, Y., et al. (2022). Improved Chan algorithm based optimum UWB sensor node localization using hybrid particle swarm optimization. *IEEE Access, 10*, 32546–32565. https://doi.org/10.1109/ACCESS.2022.3157719
7. Nosrati, L., Fazel, M. S., & Ghavami, M. (2022). Improving indoor localization using mobile UWB sensor and deep neural networks. *IEEE Access, 10*, 20420–20431. https://doi.org/10.1109/ACCESS.2022.3151436
8. Coppens, D.A. (2022). An overview of UWB standards and organizations (IEEE 802.15.4, Fira, Apple): Interoperability aspects and future research directions. *IEEE Access, 10*, 70219–70241. https://doi.org/10.1109/ACCESS.2022.3187410
9. Lee, G., et al. (2022). An IR-UWB CMOS transceiver with extended pulse position modulation. *IEEE Journal of Solid-State Circuits, 57*(8), 2281–2291. https://doi.org/10.1109/JSSC.2022.3178668
10. Naseri, M., et al. (2022). Machine learning-based angle of arrival estimation for ultra-wide band radios. *IEEE Communications Letters, 26*(6), 1273–1277. https://doi.org/10.1109/LCOMM.2022.3167020
11. Yin, Z., et al. (2019). WUB-IP: A high-precision UWB positioning scheme for indoor multiuser applications. *IEEE Systems Journal, 13*(1), 279–288. https://doi.org/10.1109/JSYST.2017.2766690
12. Liu, R., et al. (2022). Cost-effective mapping of mobile robot based on the fusion of UWB and short-range 2-D LiDAR. *IEEE/ASME Transactions on Mechatronics, 27*(3), 1321–1331. https://doi.org/10.1109/TMECH.2021.3087957
13. Phasukkit, P. (2022). Non-ionic deep learning-driven IR-UWB multiantenna scheme for breast tumor localization. *IEEE Access, 10*, 4536–4549. https://doi.org/10.1109/ACCESS.2021.3140083
14. Otim, T., et al. (2020). Towards sub-meter level UWB indoor localization using body wearable sensors. *IEEE Access, 8*, 178886–178899. https://doi.org/10.1109/ACCESS.2020.3027669
15. Dumphart, G., et al. (2022). Pairwise node localization from differences in their UWB channels to observer nodes. *IEEE Transactions on Signal Processing, 70*, 1576–1592. https://doi.org/10.1109/TSP.2022.3150951
16. Stoica, L., et al. (2005). An ultrawideband system architecture for tag based wireless sensor networks. *IEEE Transactions on Vehicular Technology, 54*(5), 1632–1645.
17. Milanovic, J., et al. (2015). Method for bandwidth efficiency increasing of M-ary PPM transmitted-reference UWB communication systems. *Wireless Personal Communications, 83*, 1927–1944. https://doi.org/10.1007/s11277-015-2495-y
18. Ma, H., et al. (2020). Design of a superposition coding PPM-DCSK system for downlink multi-user transmission. *IEEE Transactions on Vehicular Technology, 69*(2), 1666–1678. https://doi.org/10.1109/TVT.2019.2958418
19. Alabd, M. B., et al. (2022). Modified pulse position modulation for joint radar communication based on chirp sequence. *IEEE Microwave and Wireless Components Letters, 32*(10), 1247–1250. https://doi.org/10.1109/LMWC.2022.3169287
20. Xu, Z., et al. (2014). On the nonlinear Teager–Kaiser operator for energy detection based impulse radio UWB receivers. *IEEE Transactions on Wireless Communications, 13*(5), 2955–2965.
21. Xu, Z., et al. (2012). Nonlinear blind narrowband interference mitigation for energy detection based UWB receivers. *IEEE Communications Letters, 16*(10), 1596–1599.
22. Khani, H., & Azmi, P. (2009). Weighted high data rate UWB-TR system in dense multipath fading channels. *IET Communications, 3*(4), 571–584.

23. Wu, L., Wu, X., & Tian, Z. (2006). Asymptotically optimal UWB receivers with noisy templates: Design and comparison with rake. *IEEE Journal on Selected Areas in Communications, 24*(4), 808–814.
24. Hassan, N., et al. (2022). ERPPM IoNT: Event recognition using pulse position modulation in internet of nano things. *Nano Communication Networks, 31*, 100393. https://doi.org/10.1016/j.nancom.2022.100393
25. Singh, P., & Jung, S.-Y. (2022). Multi-level pulse position modulation scheme for enhancing link capacity in electromagnetic nanocommunication networks. *ICT Express, 8*(4), 633–639. https://doi.org/10.1016/j.icte.2022.07.011
26. Taki, H., et al. (2019). On optimizing the performance of impulse radio pulse position modulation based on UWB gaussian pulse derivatives. In: *Fourth international conference on advances in computational tools for engineering applications (ACTEA)*, pp. 1–5 (2019). https://doi.org/10.1109/ACTEA.2019.8851077
27. Singh, P., & Jung, S.-Y. (2022). Performance analysis of time-hopping multiple access using multilevel PPM for terahertz nanocommunications. *IEEE Transactions on Nanotechnology, 21*, 810–822. https://doi.org/10.1109/TNANO.2022.3226760
28. Singh, P., & Jung, S.-Y. (2022). Multilevel pulse position modulation with level trimming for electromagnetic nanocommunications in the terahertz band. *IEEE Access, 10*, 94158–94168. https://doi.org/10.1109/ACCESS.2022.3204044
29. Abou-Rjeily, C. (2017). On the design of maximal-rate shape-preserving 2×2 and 3×3 space-time codes for noncoherent energy-detection-based PPM communications. *IEEE Transactions on Wireless Communications, 16*(11), 7432–7445. https://doi.org/10.1109/TWC.2017.2748587
30. Abou-Rjeily, C. (2016). Permutation-based noncoherent space-time codes with analog energy detection for IR-UWB communications with PPM. *IEEE Transactions on Wireless Communications, 15*(8), 5541–5554. https://doi.org/10.1109/TWC.2016.2561282
31. Simon, M. K., & Vilnrotter, V. A. (2003). Multi-pulse pulse-position-modulation signaling for optical communication with direct detection. IPN Progress Report 42-155, Jet Propulsion Laboratory, California Institute of Technology, California (2003)
32. Chen, L. (2014). An enhanced pulse position modulation (PPM) in ultra-wideband (UWB) systems. Master's thesis, University of Northern Iowa
33. Shi, X., et al. (2021). BER performance analysis of non-coherent Q-ary pulse position modulation receivers on AWGN channel. *Sensors, 21*(18), 6102. https://doi.org/10.1007/10.3390/s21186102
34. Lee, G., et al. (2022). An IR-UWB CMOS transceiver with extended pulse position modulation. *IEEE Journal of Solid-State Circuits, 57*(8), 2281–2291. https://doi.org/10.1109/JSSC.2022.3178668
35. Kim, J., & Clerckx, B. (2022). Wireless information and power transfer for IoT: Pulse position modulation, integrated receiver, and experimental validation. *IEEE Internet of Things Journal, 9*(14), 12378–12394. https://doi.org/10.1109/JIOT.2021.3135712
36. Gishkori, S., & Leus, G. (2013). Compressive sampling based energy detection of ultra-wideband pulse position modulation. *IEEE Transactions on Signal Processing, 61*(15), 3866–3879. https://doi.org/10.1109/TSP.2013.2260747
37. Magaña, M. E., Liu, H., & Venkatesan, V. (2012). Performance of a binary PPM ultra-wideband communication system with direct sequence spreading for multiple access. *Wireless Personal Communications, 65*, 125–142. https://doi.org/10.1007/s11277-011-0231-9
38. Huyen, N. T., Le Cuong, N., & Thanh Hiep, P. (2020). Proposal of UWB-PPM with additional time shift for positioning technique in nondestructive environments. *Applied Sciences, 10*(17), 6011. https://doi.org/10.3390/app10176011
39. Ramirez-Mireles, F. (2012). Some M-ary sequence designs for pulse-based UWB and other systems based on PPM. *Wireless Personal Communications, 63*, 129–145. https://doi.org/10.1007/s11277-010-0111-8
40. Wang, Z., et al. (2021). Real-time bidirectional transmission of up to 1.25-gbps 16-PPM over a free-space optical link. In: *Asia communications and photonics conference (ACP)*, pp. 1–3
41. Dixit, V., & Kumar, A. (2021). Error analysis of L-PPM modulated ADT based VLC system with perfect and imperfect CSI. In: *International conference on control, automation, power and signal processing (CAPS)*, pp. 1–6. https://doi.org/10.1109/CAPS52117.2021.9730708
42. Wang, Y., et al. (2022). Research on transmission rate of deep space optical communications based on PPM technology. In: *2nd international conference on consumer electronics and computer engineering (ICCECE)*, pp. 356–359. https://doi.org/10.1109/ICCECE54139.2022.9712825
43. Cao, T., et al. (2023). Performance of multipulse pulse-position modulation in NLOS ultraviolet communications. *IEEE Communications Letters, 27*(3), 901–905. https://doi.org/10.1109/LCOMM.2023.3236613

44. Li, R., et al. (2022). Optimal pulse-position modulation order and transmit power in covert communications. *IEEE Transactions on Vehicular Technology, 71*(5), 5570–5575. https://doi.org/10.1109/TVT.2022.3151197
45. Richardson, P. C., Xiang, W., & Stark, W. (2006). Modeling of ultra-wideband channels within vehicles. *IEEE Journal on Selected Areas in Communications, 24*(4), 906–912.

Hassan Khani received the B.Sc. degree from the Ferdowsi University of Mashhad, Mashhad, Iran, in 2002, and the M.Sc. and Ph.D. degrees from the Tarbiat Modares University, Tehran, Iran, in 2005 and 2010, respectively, all in electrical engineering. From 2003 to 2005, he was with the Signal Processing Research Group at the Iran Telecommunication Research Center, Tehran, Iran. From 2006 to 2007, he was with the Advanced Communications Research Institute, Sharif University of Technology, Tehran, Iran. From 2008 to 2010, he was with the Electrical and Computer Engineering (ECE) Department, Quchan University of Technology (QUT), Quchan, Iran. From 2011 to 2013, he was a Postdoctoral Fellow/Research Scientist at the Department of Industrial Technology, University of Northern Iowa, Cedar Falls, IA, USA. He is currently an Assistant Professor with the ECE Department of QUT. His current research interests include modulation and coding techniques, signal processing, and ultra-wideband communications.